The Astrophysical Journal, 607:333–341, 2004 May 20
© 2004. The American Astronomical Society. All rights reserved. Printed in U.S.A.

A NEW MEASUREMENT OF THE INTENSITIES OF THE HEAVY PRIMARY COSMIC-RAY NUCLEI AROUND 1 TeV amu^{-1}

F. Gahbauer,[1] G. Hermann,[2] J. R. Hörandel,[3] D. Müller, and A. A. Radu[4]
Enrico Fermi Institute, University of Chicago, 933 East 56th Street, Chicago, IL 60637
Received 2003 December 6; accepted 2004 February 3

ABSTRACT

We describe a new measurement of the intensities of the heavy primary cosmic-ray nuclei O, Ne, Mg, Si, and Fe from 10 GeV amu^{-1} to energies beyond 1 TeV amu^{-1}. The measurement was conducted in 1999 during a 1 day test flight of the Transition Radiation Array for Cosmic Energetic Radiation (TRACER), a new cosmic-ray telescope designed for long-duration balloon flights. TRACER uses an array of thin-walled single-wire proportional tubes to determine the particle Lorentz factor from measurements of specific ionization and transition radiation. The nuclear charge is obtained with plastic scintillators, and low-energy background is identified with an acrylic Cerenkov counter. The results of this observation are consistent with previous measurements in this energy region. The current statistical limitations should be greatly improved with the planned long-duration exposure of TRACER.

Subject headings: balloons — cosmic rays — instrumentation: detectors — ISM: abundances

1. INTRODUCTION

While the overall cosmic-ray intensity covers an enormous range of energies, extending beyond 10^{20} eV per particle, details on the composition of the cosmic rays are known for only a fraction of this range. Yet without information on the abundances and energy spectra of the individual cosmic-ray components, conclusions about the sources of these particles, and of their acceleration and transport through the galaxy, remain tentative and often controversial. Particularly important, but difficult to identify at high energies, are the cosmic-ray nuclei heavier than protons and helium. These include primary nuclei that are generated by nucleosynthesis and subsequently accelerated in cosmic-ray sources, as well as secondary nuclei, produced by spallation in the interstellar medium.

Currently, measurements of the energy spectra and absolute intensities of these individual elemental species extend to a few TeV amu^{-1} (or total energies around several 10^{13} eV per nucleus) for the major primary nuclei (Grunsfeld et al. 1988; Müller et al. 1991), and up to $\sim$0.2 TeV amu^{-1} for some of the secondary nuclei (Binns et al. 1988; Engelmann et al. 1990; Swordy et al. 1990). These measurements support a model in which all cosmic-ray nuclei are accelerated with the same differential energy spectrum in the form of a power law in energy, $E^{-\gamma}$, with power-law index $\gamma \approx 2.1-2.2$ at the source. This value of the power-law index γ is close to that expected if acceleration in strong shocks, probably from supernovae, provides the main mechanism to generate the particles. Even at the highest energies, the relative abundances of the primary nuclei at the source (Müller et al. 1991) show the same anticorrelation with first ionization potential or with volatility that is observed at lower energies (Meyer 1985) and for solar energetic particles (Reames 1995).

The shape of the source energy spectrum has been inferred from local measurements, taking into account that the propagation path length Λ of the cosmic rays through the galaxy decreases with energy as $\Lambda^{-\alpha}$, $\alpha \approx 0.6$ (Swordy et al. 1993). The energy dependence of propagation causes the energy spectra observed near Earth to be considerably softer than those at the cosmic-ray sources. It is important to realize that this model of cosmic-ray propagation is supported by data only over a rather restricted region of energies: below a few GeV amu^{-1}, solar modulation obscures the interstellar energy spectra, and beyond $\sim$100 GeV amu^{-1}, the propagation path length is unknown. Beyond 1000 GeV amu^{-1}, even for the primary nuclei, at most the energy spectra of groups of elements have been determined in direct measurements above the atmosphere (Takahashi et al. 1998; Apanasenko et al. 2001). At still higher energies, indirect observations of cosmic-ray air showers may permit the determination of the *mean mass* of the particles but have not yet led to an undisputed result (Swordy et al. 2002; Hörandel 2003). In some air shower observations such as KASKADE (Antoni et al. 2003), a great deal of information is available, but the interpretation is limited because of uncertainties in high-energy nuclear interaction models (Antoni et al. 2002).

There are good reasons to question whether the decrease of the propagation path length continues much beyond presently measured energies. One also expects that the supernova shock acceleration mechanism will become inefficient in the 10^{14}–10^{15} eV per particle region (Lagage & Cesarsky 1983). Thus, there is a great deal of uncertainty and speculation about the nature of cosmic rays beyond the TeV-per-amu regime. Extending reliable measurements to higher energies represents a severe experimental challenge. The present work is motivated by this challenge.

2. EXPERIMENTAL APPROACH

Because of the rapidly decreasing cosmic-ray intensity at high energies, observations require instruments with large collection power. For instance, to detect the heavy primary nuclei in the energy region $10^{14}-10^{15}$ eV per particle with reasonable statistics, a collecting power of several hundred

[1] Current address: Columbia Astrophysics Laboratory, New York.
[2] Current address: Max-Planck-Institut für Kernphysik, Heidelberg.
[3] Current address: Institut für Experimentelle Kernphysik, Universität Karlsruhe.
[4] Current address: Institute for Space Sciences, Bucharest, Romania.

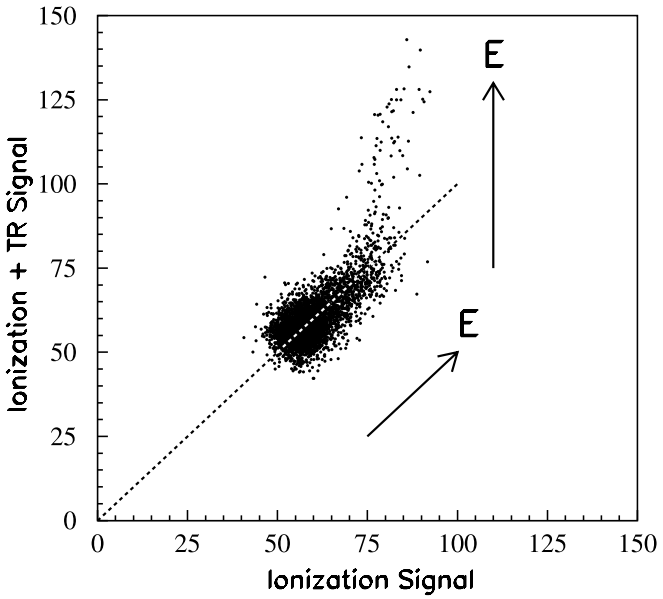

FIG. 1.—Simulation of detector response. Fe nuclei with a differential energy spectrum $\propto E^{-1.7}$ are assumed to traverse a detector such as shown in Fig. 2, which independently measures the ionization signal in gas layers, and the ionization signal, superposed with TR X-rays. The cross-correlation of simulated individual events in both detectors is shown in arbitrary units. Events are expected to cluster along the dashed line if the signals had the same magnitude in both detectors. The arrows qualitatively indicate the direction of increasing particle energy.

m^2 sr days may be needed. This requirement is very difficult to satisfy above the atmosphere with traditional calorimeters or magnet spectrometers. Hence, we choose transition radiation detectors (TRDs) to measure the particles' Lorentz factor $\gamma = E/mc^2$. They are combined with plastic scintillators and gas proportional counters that record the specific ionization and identify the individual elemental species by their charge number Z. A TRD does not require a nuclear interaction to take place; it consists of radiators and X-ray detectors that have low weight per unit area. TRDs were first used in this fashion by the cosmic ray nuclei detector (CRN) flown on the space shuttle *Challenger* in 1985 (L'Heureux et al. 1990). The instrument described here, TRACER (Transition Radiation Array for Cosmic Energy Radiation), does, in many ways, benefit from the heritage of CRN.

The CRN instrument had used radiators of plastic fibers to generate TR X-rays, and thin-window multiwire proportional chambers (MWPCs) to detect the X-rays. The MWPCs operated at atmospheric pressure with a gas mixture containing 25% xenon. The entire instrument was therefore enclosed in a gas-tight gondola and kept at atmospheric pressure. For TRACER, we employ the same radiator configuration that was used in CRN. However, the MWPCs are replaced by arrays of single-wire proportional tubes as X-ray detectors. Even though they are made of thin-walled aluminized mylar, they can easily withstand internal overpressures up to several atmospheres. Hence, a pressurized gondola is not needed for TRACER, significantly decreasing the detector weight and making it commensurate with the constraints for balloon-borne instruments.

The design of the TRD is tuned to provide an energy-dependent (i.e., γ-dependent) X-ray signal for Lorentz factors γ above about 500. The signal then reaches saturation for γ-values of a few times 10^4 (L'Heureux et al. 1990; Wakely et al. 2004). It is detected in the proportional tubes, superposed on the ionization signal of the particle. Although the TR signal scales with Z^2, it is important to realize that the signal is not large and is superposed on the ionization signal of the primary particle. Great care must then be taken that the abundant background of low-energy nuclei does not lead to occasional event signatures that mimic a high-energy particle in the TR region. These backgrounds are rejected by several means:

1. For both CRN and TRACER, we have repeated layers of radiator/detector pairs which provide several independent measurements of the TR signal. For an accepted event, these measurements must be consistent with each other.
2. The TR signal is evaluated along the particle trajectory through the detector. Spurious background signals from the detector area away from the trajectory can therefore be ignored. Because of the tube structure, the particle trajectory can be obtained for TRACER with higher accuracy than was possible for CRN.
3. We perform an independent measurement in order to reject low-energy particles. For CRN, this was done with the addition of a pair of gas-Cerenkov counters having a threshold Lorentz factor of $\gamma \sim 40$. In TRACER, we employ an array of gas-filled proportional tubes that identify minimum ionizing particles on the basis of their ionization signals, and that estimate the energy of each cosmic-ray nucleus of higher energy (but below the TR-region) from the relativistic rise in the specific ionization. Figure 1 illustrates the power of simultaneous measurements of ionization energy loss, and of ionization energy loss with superposed TR.

The figure shows the correlation between these two quantities for a Monte Carlo simulation of iron nuclei with a power-law spectrum of energies. The simulation uses a realistic model, with the correct response functions for the TRACER instrument described in more detail below. At low energies, both signals increase along the diagonal. At energies between 500 and 1000 GeV per nucleon, the ionization energy loss signal begins to saturate, while the TR signal begins to rise steeply. Thus, the highest energy events deviate from the diagonal near the saturation level of the ionization energy loss, with energy increasing toward the top of the figure. This feature permits a unique identification of highly relativistic particles, provided the intrinsic fluctuations of the signals are sufficiently small. Finally, TRACER employs an acrylic Cerenkov counter in order to reject low-energy particles that generate enhanced ionization signals because their energy is below the minimum ionization region. We emphasize that the steeply falling cosmic-ray energy spectrum necessitates that all of these techniques be employed in order to measure the Lorentz factor of a high-energy cosmic-ray nucleus without ambiguity.

3. DESCRIPTION OF THE INSTRUMENT

The TRACER instrument is shown schematically in Figure 2. It is designed for one or several circumpolar balloon flights, each of about 2 weeks' duration. Plastic scintillators for charge measurement are located at the top and bottom of the instrument. They also serve to trigger the instrument. An acrylic Cerenkov counter that rejects low-energy background particles is mounted below the bottom scintillator. A proportional tube array and TRD, employing a total of 1584 single-wire proportional tubes, are at the center of the instrument. Half of these tubes measure the ionization energy loss only, while the

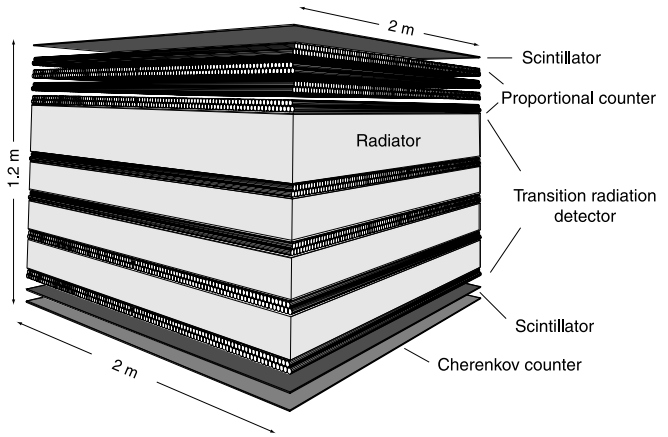

FIG. 2.—Cross section of the TRACER detector system

remainder is interspersed with four radiator layers to generate TR for the most energetic nuclei.

Both plastic scintillators are 0.5 cm thick and are divided into four quadrants of 1 m^2 area each, as shown in Figure 3. Wavelength shifter bars collect the light exiting the edge of the scintillator and direct the reemitted light to photomultiplier tubes (PMTs). One PMT is connected to each wavelength shifter bar. The design of the Cerenkov counter is similar, except that the thickness is 1.27 cm, and that there are two PMTs mounted on opposite ends of each wavelength shifter bar. The last dynode signals from each of the PMTs are individually integrated, analyzed with 12 bit resolution by peak-detecting ADCs, and recorded for each event. The anode signals from the scintillator PMTs are summed for each scintillator and passed via discriminators to a coincidence trigger.

The proportional tubes are 2 m long and have a diameter of 2 cm. They are filled in-flight with a xenon-methane mixture at half an atmosphere. As can be seen in Figure 2, the tubes are arranged in eight double layers that are oriented in two orthogonal directions. This arrangement permits three-dimensional tracking of the particle through the instrument. The top layers form the proportional tube array and measure ionization energy loss, while the lower layers detect ionization energy loss plus any superposed TR signal.

The signals from the proportional tubes are amplified individually by the AMPLEX circuit (Beuville et al. 1990), which packages 16 amplifier channels on a single integrated circuit. The amplified signals are digitized with 8-bit resolution. The dynamic range of the AMPLEX amplifier is not sufficient to cover the entire charge range from lithium to iron. Therefore, for the present configuration, the trigger threshold is set between carbon and oxygen, which allows for all elements from oxygen to iron to be studied. To reduce the data rate, the readout electronics only accepts proportional tube signals that exceed the pedestal level by an adjustable threshold.

The pulse heights from the PMTs and the proportional tubes are formatted into an event, which is stored on-board on a hard disk and is also sent to the ground via telemetry. Specially formatted "housekeeping events," which contain information about the status of the instrument, are included periodically. A telemetry bandwidth of 455 kbit s^{-1} is available when the balloon is in line-of-sight range and can easily handle the data rate. More detail on the construction and performance of the detector subsystems will be described in a separate paper.

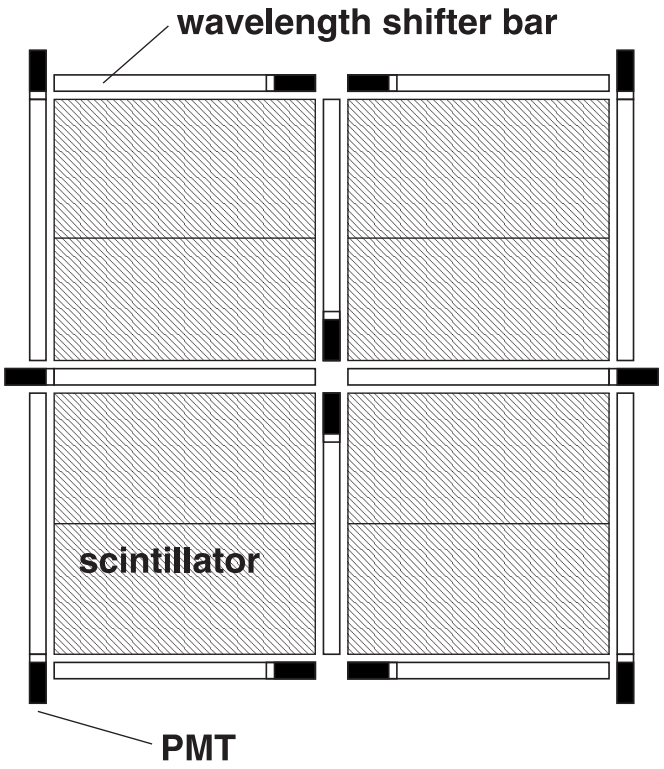

FIG. 3.—Schematic arrangement (not to scale) of scintillator sheets, wavelength shifter bars, and PMTs.

Before a long-duration balloon flight could be conducted, TRACER was subjected to a 1 day test flight. It was launched from Fort Sumner, New Mexico, on 1999 September 20. The balloon floated for about 28 hr at an altitude between 34 and 38 km, corresponding to a residual atmospheric depth between 3.3 and 6.5 g cm^{-2}. The geomagnetic cutoff varied between 4.4 and 4.8 GV during the flight. The results from this flight are presented in the following.

4. DATA ANALYSIS

4.1. *Overview*

After the signals are corrected for gain and pedestal variations, the first step of the data analysis is to reconstruct the trajectory of each particle through the instrument. Accurate trajectory information is needed to correct for spatial variations in the scintillator and Cerenkov counter responses, and to determine the path length of the particle through the cylindrical proportional tubes. From the corrected scintillator signals, a nuclear charge Z is assigned to each cosmic-ray nucleus. We require consistent charge measurements in both the top and bottom scintillators in order to reject nuclei that have interacted in the material of the instrument. Based on signals from the TRD tubes, dE/dx tubes, and Cerenkov counter, each nucleus is then assigned to an energy interval. Finally, we compute the absolute flux, taking into account not only the energy resolution and nonlinear energy response of the detector, but also efficiency losses due to atmospheric interactions or interactions in the instrument, and due to the various selection cuts in the analysis.

4.2. *Trajectory Reconstruction*

To first order, the trajectory of each particle is determined by fitting a line to the centers of all collinear tubes showing

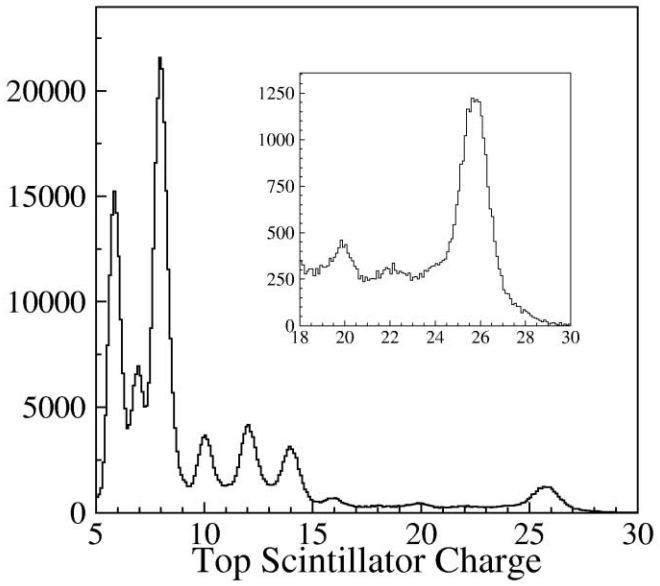

FIG. 4.—Charge histogram for the top scintillator measured in flight. Note that the trigger threshold suppresses charges with $Z \leq 6$.

signals in response to the particle. The initial trajectory is improved by assuming that the energy deposit in each tube is proportional to the path length in that tube. As a final refinement, we use a likelihood method to determine the most likely trajectory assuming typical signal distributions in each tube. Monte Carlo simulations of this procedure show that the total path length of iron nuclei in the detector determined in this fashion is accurate to 2%. This error is small compared to the intrinsic signal fluctuations.

4.3. *Charge Identification*

The charge is determined in both top and bottom scintillators from the average of the square root of the signals of the four PMTs observing the quadrant through which the particle passed. A response map generated with muon signals on the ground, and refined with cosmic-ray data in flight, encapsulates spatial variations in the light collected in each PMT. The corrected PMT signals are then normalized to the inclination of the trajectory of the nucleus ("cos θ-correction") and adjusted for non-linearities in the scintillator response, which occur for high charges, $Z \geq 10$, because of large ionization densities. This leads to charge distributions as shown in Figure 4 for the top scintillator. The charge resolution in the top scintillator is 0.33 charge units for oxygen and 0.64 charge units for iron. In conjunction with an independent measurement in the bottom scintillator, the composite charge resolution improves to 0.23 and 0.48 charge units, respectively.

The signal in the top scintillator depends negligibly on energy. In the bottom scintillator, the signal increases with energy up to primary particle energies of $\sim$10 GeV amu^{-1}, because of δ-rays produced by the primary particle in the instrument, but reaches saturation beyond that energy. This is illustrated in Figure 5, which shows a scatter plot of top and bottom scintillator signals versus the Cerenkov signals: As the Cerenkov signal increases with energy, one clearly observes a corresponding increase in the bottom scintillator signal due to δ-rays.

The δ-rays also affect the Cerenkov counter, extending the region over which the Cerenkov signal increases with energy

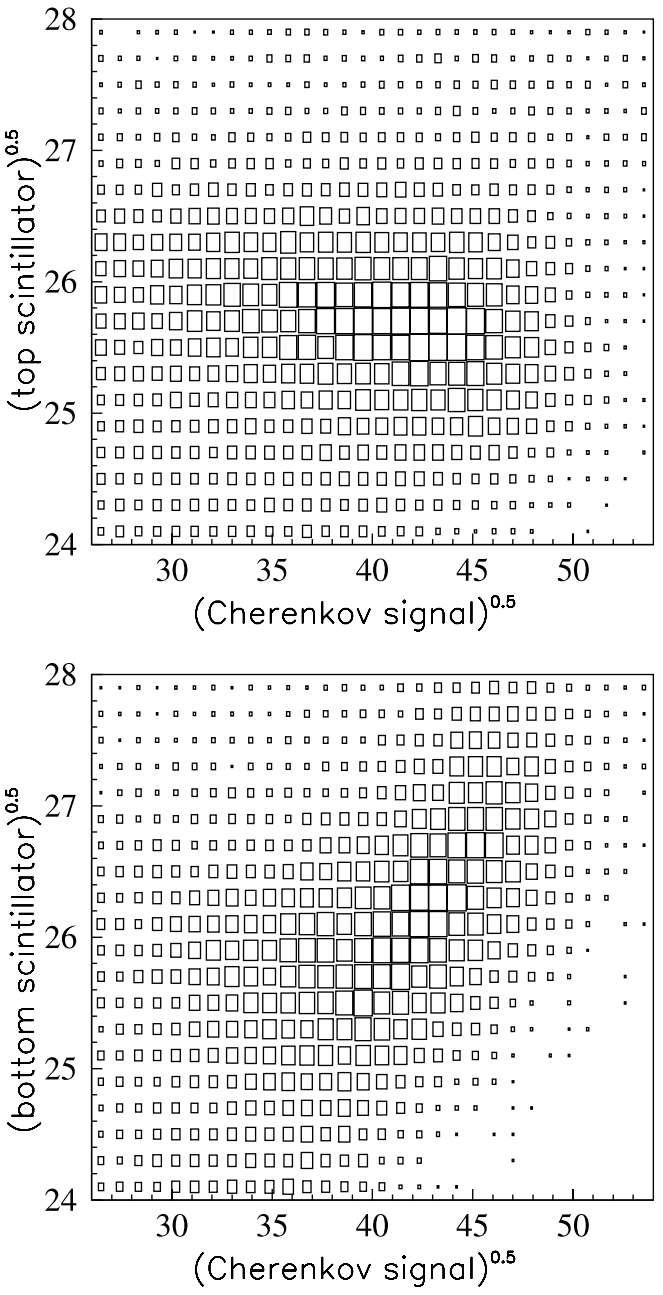

FIG. 5.—Scatter plot of signals measured in the top and bottom scintillators, respectively, vs. the signal in the Cerenkov counters for the iron nuclei. Note that the axes depict the square roots of the signals, in arbitrary units.

to $\sim$50 GeV amu^{-1}. These effects are quantitatively verified by Monte Carlo calculations and must be taken into account to avoid an energy-dependent selection efficiency in the charge cut (Gahbauer et al. 2003).

4.4. *Energy Assignment*

The design of TRACER calls for the TRD tubes to measure particle energies above $\sim$500 GeV amu^{-1}. The measurements of the Cerenkov light yield and of the ionization energy loss, dE/dx, are primarily made to reject the large background of low-energy nuclei, but they also provide energy measurements below 500 GeV amu^{-1} with moderate resolution. For the short duration of the test flight of TRACER, not many events in the TR region can be expected; therefore, these additional energy

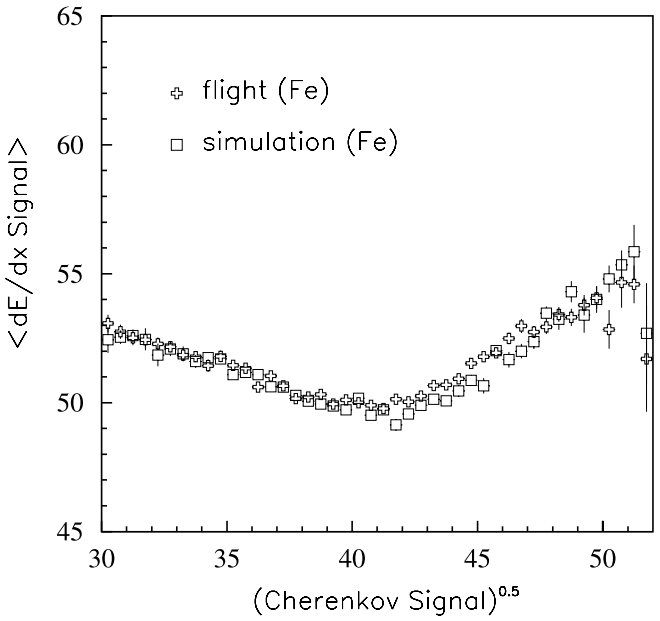

FIG. 6.—Average ionization signal measured in the proportional tubes for iron nuclei vs. the Cerenkov signal, in arbitrary units. The measurement is compared with results from a computer simulation. The minimum of the data points corresponds to the energy of minimum ionization.

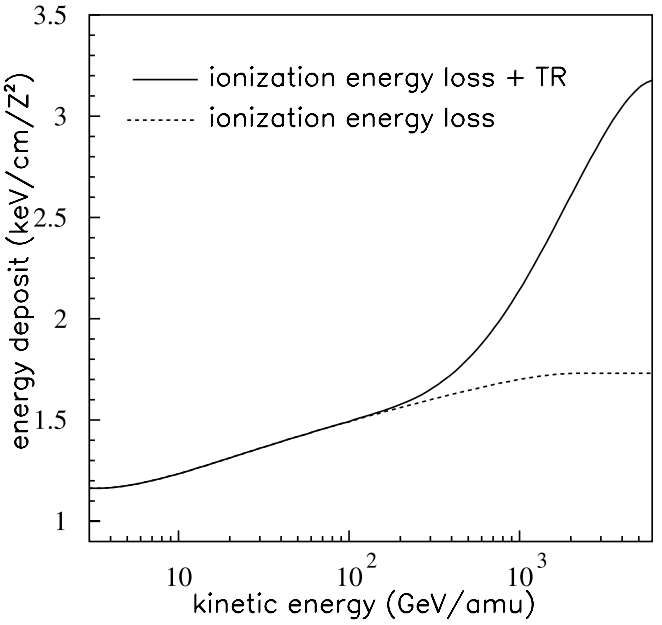

FIG. 7.—Energy response curves (in keV cm^{-1} Z^{-2}) for proportional counter tubes (ionization only) and TRD tubes (ionization+TR). Note the zero offset in the vertical scale.

measurements are a valuable by-product. To understand the energy dependence of these signals in detail, we perform Monte Carlo simulations of the instrument using GEANT 4 (Agostinelli et al. 2003) supplemented by our own codes. As mentioned above, these simulations also indicate that for the Cerenkov counter, the production of δ-rays in the instrument significantly modifies the energy response of the Cerenkov signal.

We simulate the relativistic rise of the ionization energy loss using the photoabsorption ionization model as implemented in GEANT 4 (Apostolakis et al. 2000) and check and adjust the energy response with data from the flight. The validity of the simulation is verified by two correlations:

First, we compare the average ionization energy loss signal in the proportional tubes with the Cerenkov signal, as shown in Figure 6 for iron nuclei.

The figure shows results from both flight data and simulations. This comparison normalizes the conversion of ADC counts to energy deposit in the region where the Cerenkov signal depends on energy, i.e., for $E < 50$ GeV amu^{-1}. Second, the Fermi plateau, i.e., the level at which the ionization energy loss saturates, is determined in the data from a scatterplot of TR data versus specific ionization, similar to the one shown in Figure 1. Thus, the response curve is calibrated and verified self-consistently with flight data.

We determine the response of the TRD using calculations that approximate the plastic-fiber radiators as regularly spaced foils, and using accelerator calibrations with singly charged particle beams of known Lorentz factor (L'Heureux et al. 1990; Wakely et al. 2004). The combined response curve, depicting both the relativistic rise in specific ionization and the superposed TR signal, is shown in Figure 7. The figure also shows the response curve for the proportional counter tubes (top eight layers in Fig. 2), which only measure the specific ionization.

Events with significant TR yield are identified visually on a scatterplot of TRD tube signals versus dE/dx tube signals, as shown in Figure 8 for neon and iron from the flight. The events are assigned an energy according to the response curve shown in Figure 7.

Although the number of such events is very small, the scatterplots are remarkably free of background, which gives a great degree of confidence that TR candidates are indeed identified correctly. The highest energy iron event carries a total energy of about 5×10^{13} eV.

4.5. *Energy Deconvolution*

Care must be taken when reconstructing energy spectra from measurements using detectors with finite energy resolution. The energy resolution is a function of charge and energy. For example, the energy resolution for iron $\Delta E/E$ is +46%–25% in the Cerenkov region around 3 GeV amu^{-1}, +90% and −50% in the relativistic rise region around 20 GeV amu^{-1}, and ±20% in the TRD region around 1000 GeV amu^{-1}.

The response functions, such as the ones shown in Figure 7 for the proportional counter tubes and the TRD, are used to assign an energy to each event and to group the events into energy intervals (see Table 1). Because of the steeply falling spectrum, signal fluctuations make it more likely to assign a low-energy event incorrectly to a high-energy bin than the other way around. To understand this effect and correct for it, we use simulations that determine the impact of the detector's finite energy resolution on the reconstructed spectrum for different assumed forms of the true spectrum. If the bin sizes are sufficiently wide, corresponding to at least 2 σ in energy resolution, a simple correction factor consisting of the ratio of the true number of events in a given energy bin to the measured number can be obtained from the simulations. This factor does not depend strongly on the assumed input spectrum and can be refined by iteration. We use these overlap corrections for energy measurements from the Cerenkov signals and from the ionization energy loss signals. For TR

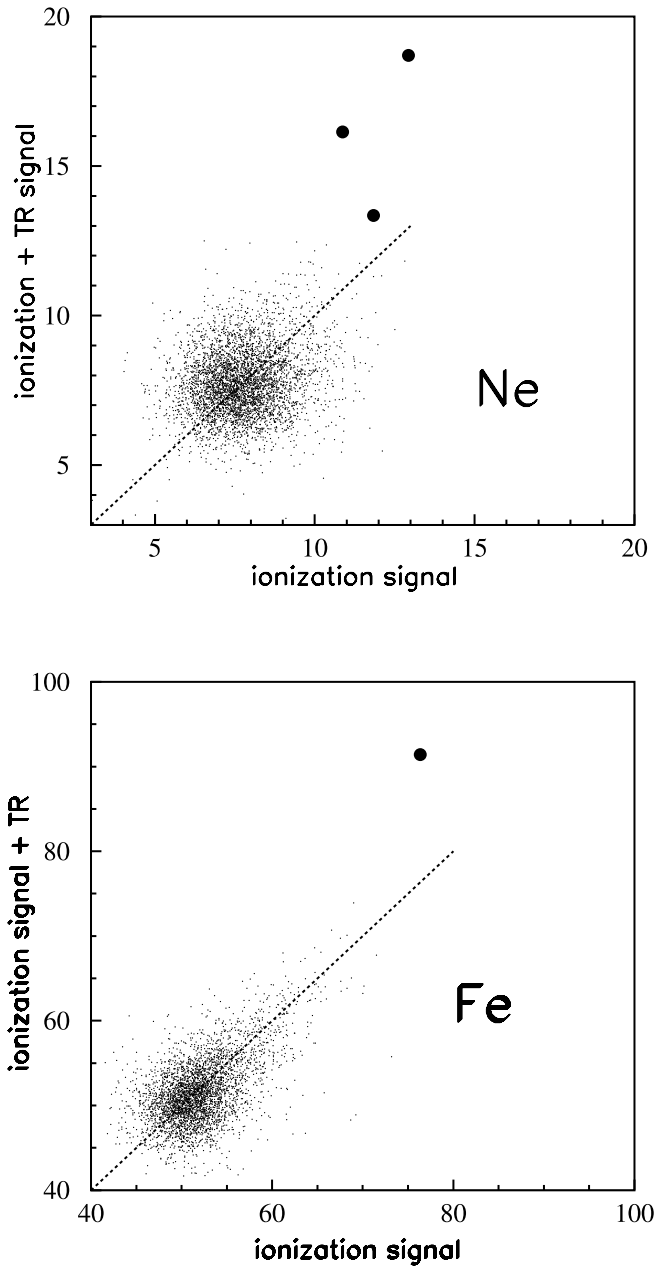

FIG. 8.—Cross-correlations between the measured TRD signals and the measured specific ionization in the proportional tube array for neon and iron nuclei, respectively. These plots correspond to the simulation illustrated in Fig. 1. The scales are in arbitrary units.

signals, the energy response is quite steep, and overlap corrections are then insignificant.

4.6. *Absolute Flux Calibration*

To derive absolute fluxes from the numbers of events in each energy bin after overlap corrections, we determine the geometric aperture of the detector and the probability of particle losses due to cuts by the various selection criteria, nuclear interactions in the atmosphere or in the instrument, or dead time in the data acquisition. The overall geometric factor of TRACER is 4.42 m^2 sr, and the total exposure time is 22.6 hr. Dead-time losses are negligible for this flight. In the data analysis, we exclude events that traverse areas of the scintillators for which the spatial response is currently not well mapped. At the present state of the analysis, these amount to about 25% of the total area for each scintillator. The remaining efficiencies due to data analysis cuts are summarized for oxygen and iron in Table 2.

We emphasize that the cuts employed here are very conservative. Work is currently in progress to understand which of the criteria can be relaxed in order to improve the statistics of the results without compromising the quality of the data. Losses due to nuclear interactions are computed using a combination of measured charge-changing cross sections and parameterizations obtained by Heckman et al. (1978) and Westfall et al. (1979). The interaction losses are taken to be independent of energy but do depend on the particle charge and mass. For instance, for oxygen ($Z = 8$), we find that 79% traverse the atmosphere above the balloon without interaction, while 65% penetrate the instrument without interaction. For iron ($Z = 26$), the corresponding numbers are 64% and 50%, respectively.

5. RESULTS

Results for the energy spectra of the heavy primary cosmic-ray nuclei (O, Ne, Mg, Si, and Fe) are presented in Table 1 and Figure 9.

The data points are plotted according to the method of Lafferty & Wyatt (1995), such that the flux values, $f_i = n_i/(E_{i+1} - E_i)$, are multiplied by $E^{2.5}_{\mathrm{plot},i}$, where n_i are the number of particles observed in the energy bin from E_i to E_{i+1}, and $E_{\mathrm{plot},i}$, is the energy at which the data point is plotted. The energy value $E_{\mathrm{plot},i}$ is chosen in such a way that

$$f(E_{\mathrm{plot},i}) = \frac{1}{E_{i+1} - E_i} \int_{E_i}^{Ei+1} f(E)\, dEm, \qquad (1)$$

where $f(E)$ is the assumed differential spectrum. For the lowest energy point, which covers a wide energy interval in which the spectral slope changes, the shape of the spectrum is adapted from the measurements on HEAO (Engelmann et al. 1990). For the higher energies, we assume $f(E) = E^{-2.5}$. The lowest energy data point for each element is derived from the energy dependence of the Cerenkov signal. For the $Z \geq 12$ nuclei, we derive information about the intensities at intermediate energies from the relativistic increase in the ionization signal in the proportional tubes (15 GeV $\mathrm{amu}^{-1} < E <$ 500 GeV amu^{-1}). The highest energy values for all elements are derived from the TRD signals. For comparison with the TRACER measurements, Figure 9 includes results reported by HEAO (Engelmann et al. 1990) and CRN (Müller et al. 1991).

6. DISCUSSION

The results from TRACER represent absolute intensities, without any arbitrary normalization, and the error bars are statistical. We note that the intensities agree very well with those obtained in previous observations in space on HEAO and CRN/*Spacelab-2*. Also, the spectral slopes for Fe, Si, and Mg agree quite well with those reported for the earlier space measurements. They do not suggest an unusually steep drop-off of the silicon flux. For Ne and O, the TRACER results might suggest slightly flatter (harder) spectra than observed with CRN. However, in view of the limited counting statistics, we cannot regard this difference to be significant. Overall, the results of the TRACER measurement appear to be quite consistent with the data from the previous measurements.

TABLE 1

Differential Fluxes of Primary Nuclei for different Energies

Element	Energy Range (GeV amu^{-1})	Number of Events	Overlap Correction	Exposure Factor[a] ($\times 10^{-3}$ m^2 sr s)	Kinetic Energy[b] (GeV amu^{-1})	Differential Flux[c] [$\times 10^8$ (m^2 sr s GeV amu^{-1})$^{-1}$]
O ($Z = 8$).....	10–725[d]	15184	0.37	29.3	64.9	1680 ± 13
	725–1651[e]	8	1	27.4	108	$1.97^{+0.97}_{-0.68}$
	1651–3546[e]	2	1	27.4	2390	$0.24^{+0.32}_{-0.16}$
	3546–20000[e]	2	1	27.4	7950	$0.028^{+0.037}_{-0.018}$
Ne ($Z = 10$).....	3–50[d]	4361	0.93	28.2	12.0	15240 ± 230
	810–1358[e]	1	1	25.4	1040	$0.359^{+0.825}_{-0.296}$
	1358–5000[e]	2	1	25.4	2520	$0.108^{+0.142}_{-0.070}$
Mg ($Z = 12$).....	2.93–50[d]	4935	1.01	26.4	11.9	16740 ± 240
	50–225[f]	135	0.29	20.6	101	44.6 ± 3.8
	225–750[f]	14	0.33	20.6	399	$1.80^{+0.62}_{-0.47}$
	750–2000[e]	1	0.33	20.6	1200	$0.108^{+0.14}_{-0.045}$
Si ($Z = 14$).....	3.15–50[d]	5855	0.97	33.1	12.7	13100 ± 170
	50–300[f]	177	0.53	31.8	115	32.6 ± 2.8
	300–800[f]	11	0.61	31.8	480	$1.37^{+0.58}_{-0.43}$
	800–5000[e]	1	0.67	31.8	1880	$0.018^{+0.041}_{-0.015}$
Fe ($Z = 26$).....	3–14.1[d]	3368	1.02	33.5	6.72	16480 ± 280
	14.1–37.2[f]	534	0.76	33.5	22.5	947 ± 41
	37.2–117.5[f]	123	0.78	33.5	64.3	64.2 ± 5.8
	117.5–340[f]	19	0.62	33.5	195	$2.84^{+0.81}_{-0.65}$
	340–794[f]	1	0.87	33.5	512	$0.103^{+0.236}_{-0.085}$
	794–1360[e]	1	1	33.5	1240	$0.044^{+0.10}_{-0.037}$

[a] The product of the geometric aperture, detector live time, and all efficiencies, including instrument and atmospheric interaction losses.

[b] The kinetic energy for plotting the differential flux value is computed according to the method described by Lafferty & Wyatt (1995) by assuming a constant spectral index of $E^{-2.5}$ over the whole energy interval, except in the first bin, where the HEAO data (Engelmann et al. 1990) are used to provide the spectral shape.

[c] Asymmetric errors computed according to Gehrels (1986).

[d] Energy derived from Cerenkov signal.

[e] Energy derived from TRD signal.

[f] Energy derived from relativistic rise of dE/dx signal.

Considering the general paucity of measurements at high energies, and considering the fact that the TRACER configuration is substantially different from that of previous detectors, this is a significant result. Even though the TRACER measurement does not yet extend beyond the range of previous observations, it seems to reinforce the interpretation of the earlier data: the heavy cosmic-ray nuclei up to energies in the TeV-per-amu region (or total energies well above 10^{13} eV per event) appear to be accelerated with the same power-law spectrum at the source, that is much harder, however, than the observed spectrum as a result of energy-dependent propagation.

The connection between the source energy spectrum $Q_i(E)$ of a cosmic-ray species (numbered i) and the observed spectrum $N_i(E)$ is often approximated by a "leaky-box" continuity equation,

$$Q_i(E) = \frac{N_i(E)}{\Lambda/\rho c} + N_i \sigma_i n c - \sum_{j>i} N_i \sigma_{ji} n c, \qquad (2)$$

TABLE 2

Efficiencies of Data Analysis Cuts

Parameter	Oxygen (%)	Iron (%)
Trigger efficiency.....	94	100
Charge selection.....	60	63
Cerenkov cut.....	94	100
Track fit (first level)	98	100
Track fit (second level).....	96	92
Self-consistency	55	91

where Λ is the propagation path length, ρ and n are the interstellar gas density or number density, respectively, σ_i and σ_{ji} are spallation cross sections for species (i) or for spallations ($j > i$) $\rightarrow$ (i), respectively, and c is the cosmic-ray speed, i.e., essentially the speed of light. Up to TeV-per-amu energies, a parameterization with $Q_i(E) \propto E^{-2.2}$ and $\Lambda(E) \propto E^{-0.6}$ is consistent with the data of the various measurements. However, Swordy et al. (1993) have pointed out that an extrapolation of the measurements with this model to higher energies is not consistent with the all-particle spectrum measured from the ground beyond total particle energies of 10^{14} eV. More recent measurements with the thin passive calorimeters JACEE (Takahashi et al. 1998) and RUNJOB (Apanasenko et al. 2001) reinforce this inconsistency, as they suggest that the spectra of the heavy nuclei from carbon upward are harder beyond 10^3 GeV amu^{-1} than the model would predict. A quantitative and plausible interpretation of this behavior would be found if the path length for escape from the galaxy $\Lambda(E)$ does not continue to decrease but asymptotically reaches a constant value $\Lambda_{\rm inf}$ at high energies. This is illustrated in Figure 10, where we compare the data for iron nuclei with predicted observed spectra for different assumptions about the residual path length $\Lambda_{\rm inf} \approx 0$, 0.15, and 0.5 g cm^{-2}. In all cases, a source spectrum $\propto E^{-2.2}$ was assumed.

Even though models with a finite path length for escape at high energies have been proposed long ago (e.g., Cowsik & Wilson 1973), Figure 10 illustrates that the currently available data do not have sufficient counting statistics to test a model with finite path length in detail and independently for the individual elements. It appears that one or several long-duration flights of TRACER could help to resolve this situation.

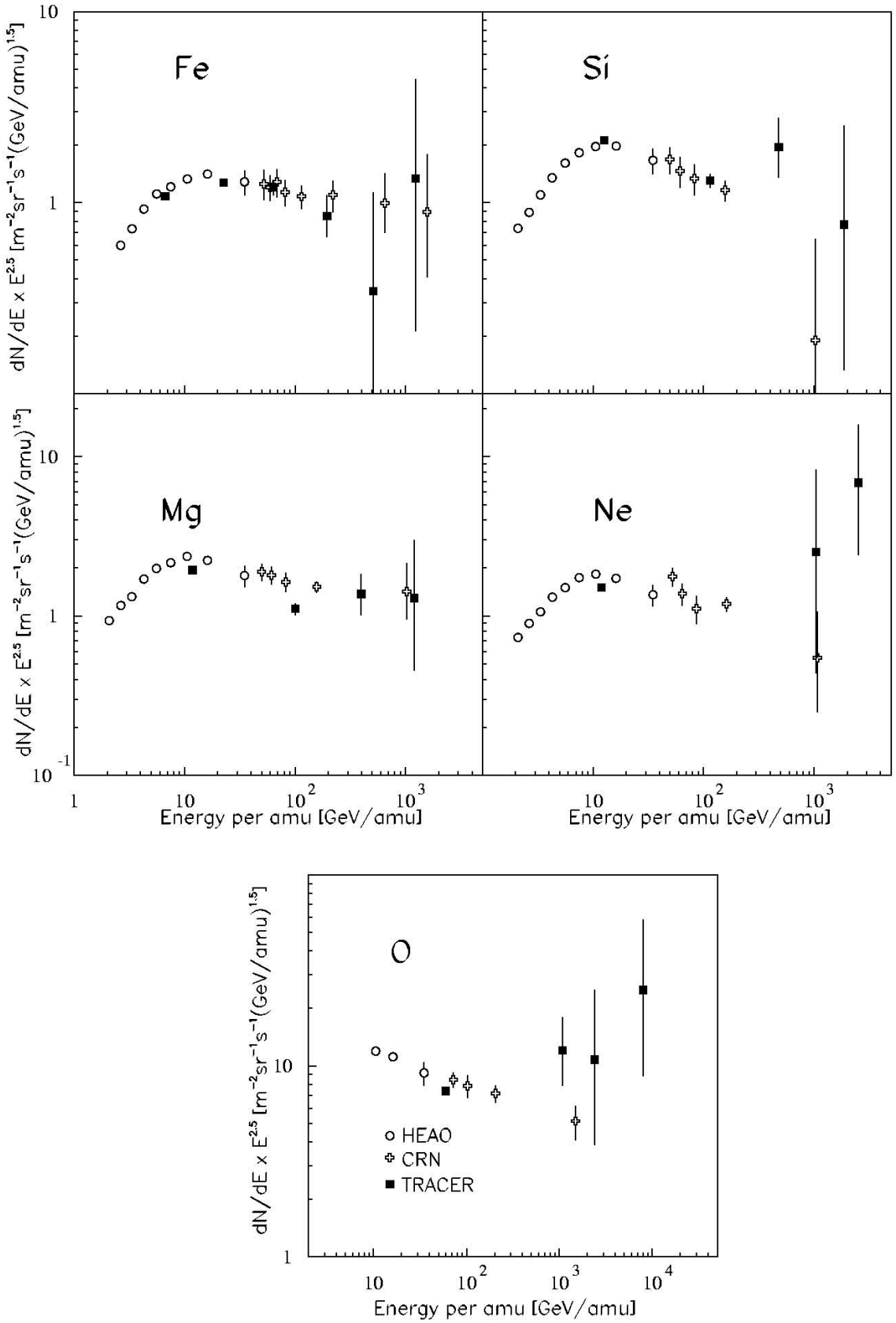

FIG. 9.—Differential energy spectra for Fe, Si, Mg, Ne, and O nuclei. The data from TRACER (*filled squares*) are compared with results from CRN (*open crosses*), and from HEAO-3 (*open circles*). Note that the intensities are multiplied with (energy per amu)$^{2.5}$.

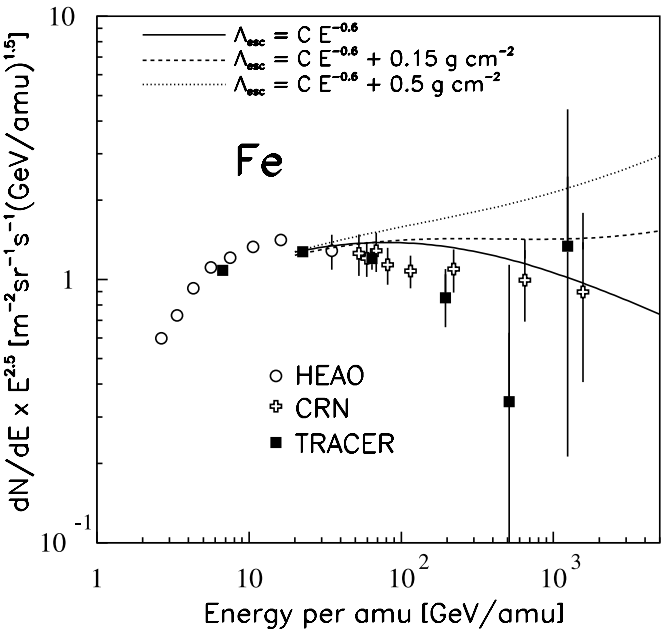

FIG. 10.—Differential energy spectrum for iron nuclei, compared with estimated spectra for different assumptions about the energy dependence of the propagation escape path length Λ_{esc}.

The long-standing question of the cosmic-ray "knee" above 10^{15} eV per particle, however, may well remain a separate mystery that most likely will not be uncovered until the measurements are extended by still another order of magnitude in energy.

7. CONCLUSION

The test flight of TRACER has verified the concept and performance of this instrument. In particular, the practicality of arrays of thin-walled proportional tubes as particle detectors in a zero-pressure environment, as well as their capability of very accurately determining the trajectory of heavy cosmic-ray nuclei through the instrument have been proven. Also, it has been shown that the combination of an acrylic Cerenkov counter and a measurement of specific ionization in gases not only provides efficient discrimination against low-energy particles (i.e., below the onset of transition radiation) but also permits measurements of particle energies over the range from a few GeV amu^{-1} to several hundred GeV amu^{-1}.

While limited in duration, the test flight has provided a new measurement of the intensities of heavy cosmic-ray nuclei up to TeV-per-amu energies. The counting statistics achieved thus far should be much improved in a long-duration balloon flight. Such a flight was scheduled for launch from McMurdo, Antarctica, in 2003 December/2004 January. Ultimately, an instrument designed similarly to TRACER should be tuned to perform measurements with good resolution up to energies in excess of 10^{15} eV per event. Such an instrument must then be flown in space for the duration of several years in order to provide the energy coverage and counting statistics that are necessary in order to address the remaining questions about galactic cosmic rays up to the knee.

We are grateful to S. Swordy for valuable advice and to S. Wakely for help with the computer simulations, and we acknowledge the excellent technical services of D. Bonasera, E. Drag, W. C. Johnson, G. Kelderhouse, B. Lynch, and D. Plitt. With support from the Aerospace Illinois Space Grant, P. Barbeau, J. Britton, and P. Hosseini have led a group of undergraduate students in many aspects of the construction and balloon flight activities of TRACER. We thank the staff of the National Scientific Balloon Facility for conducting a successful test flight. This work was supported by NASA grants NAG 5-5305 and NAG 5-5072. F. G. thanks NASA for support under the Graduate Student Researchers Program, and for support from the Aerospace Illinois Space Grant.

REFERENCES

Agostinelli, S., et al. 2003, Nucl. Instrum. Methods Phys. Res., 506, 250
Antoni, T., et al. 2002, Astropart. Phys., 16, 245
———. 2003, Nucl. Instrum. Methods Phys. Res., 513, 490
Apanasenko, A. V., et al. 2001, Astropart. Phys., 16, 13
Apostolakis, J., Giani, S., Urban, L. Maire, M., Bagulya, V. & Grichine, V. M. 2000, Nucl. Instrum. Methods Phys. Res., 453, 597
Beuville, E., Borer, K., Chesi, E., Heijne, E., Jarron, P., Lisowski, B., & Singh, S. 1990, Nucl. Instrum. Methods Phys. Res., 288, 157
Binns, W. R. Garrard, T. L., Israel, M. H., Jones, M. D., Kamionkowski, M. P., Klarmann, J., Stone, E. C., & Waddington, C. J. 1988, ApJ, 324, 1106
Cowsik, R., & Wilson, L. W. 1973, in Proc. 13th Int. Cosmic Ray Conf. (Denver), 500
Engelmann, J. J., et al. 1990, A&A, 233, 96
Gahbauer, F., Hörandel, J. R., Müller, D., & Radu, A. A. 2003, in Proc. 28th Int. Cosmic Ray Conf. (Tsukuba), 2245
Gehrels, N. 1986, ApJ, 303, 336
Grunsfeld, J. M., L'Heureux, J., Meyer, P., Müller, D., & Swordy, S. P. 1988, ApJ, 327, L31
Heckman, H. H., Greiner, D. E., Lindstrom, P. J., & Shwe, H. 1978, Phys. Rev. C, 17, 1735
Lafferty, G. D., & Wyatt, T. R. 1995, Nucl. Instrum. Methods Phys. Res., 355, 541
Lagage, P. O. & Cesarsky, C. J. 1983, A&A, 125, 249
L'Heureux, J., Grunsfeld, J. M., Meyer, P., Müller, D., & Swordy, S. P. 1990, Nucl. Instrum. Methods Phys. Res., 295, 246
Hörandel, J. 2003, Astropart. Phys., 19, 193
Meyer, J.-P. 1985, ApJS, 57, 173
Müller, D., Swordy, S. P., Meyer, P., L'Heureux, J., & Grunsfeld, J. M. 1991, ApJ, 374, 356
Reames, D. V. 1995, Adv. Space Res., 15, 41
Swordy, S. P., Grunsfeld, J., L'Heureux, J., Meyer, P., & Müller, D. 1990, Phys. Rev. D, 42, 3197
Swordy, S. P., L'Heureux, J., Meyer, P., & Müller, D. 1993, ApJ, 403, 658
Swordy, S. P., et al. 2002, Astropart. Phys., 18, 1295
Takahashi, Y., et al. 1998, Nucl. Phys. B Proc. Suppl., 60(3), 83
Wakely, S. P., Plewnia, S., Müller, D., Hörandel, J. R., & Gahbauer, F. 2004, Nucl. Instrum. Methods Phys. Res., in press
Westfall, G. D., Wilson, L. W., Lindstrom, P. J., Crawford, H. J., Greiner, D. E., & Heckman, H. H. 1979, Phys. Rev. C, 19, 1309